Colloids and Surfaces A: Physicochem. Eng. Aspects 461 (2014) 158–166

Contents lists available at ScienceDirect

Colloids and Surfaces A: Physicochemical and Engineering Aspects

journal homepage: www.elsevier.com/locate/colsurfa

Low temperature studies of the photoluminescence from colloidal CdSe nanocrystals prepared by the hot injection method in liquid paraffin

Evgenia Valcheva[a,*], Georgi Yordanov[b,**], Hideyuki Yoshimura[c], Tsvetan Ivanov[a,1], Kiril Kirilov[a]

[a] Faculty of Physics, Department of Solid State Physics and Microelectronics, Sofia University "St. Kliment Ohridski", 5 James Bourchier Blvd., 1164 Sofia, Bulgaria
[b] Faculty of Chemistry and Pharmacy, Department of General and Inorganic Chemistry, Sofia University "St. Kliment Ohridski", 1 James Bourchier Blvd., 1164 Sofia, Bulgaria
[c] Department of Physics, Meiji University, 1-1-1 Higashimita, Tama-ku, Kawasaki, Kanagava 214-8571, Japan

HIGHLIGHTS

- Low temperature studies of the photoluminescence from CdSe QDs were performed.
- Exciton photoluminescence transitions followed a modified Varshni equation.
- Thermal quenching activation energies were calculated for two temperature intervals.
- Nanoparticle growth mechanism based on Ostwald ripening is suggested.

GRAPHICAL ABSTRACT

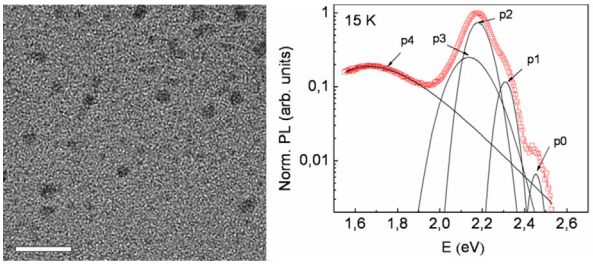

ARTICLE INFO

Article history:
Received 2 June 2014
Received in revised form 9 July 2014
Accepted 21 July 2014
Available online 5 August 2014

Keywords:
CdSe
Nanocrystals
Quantum dots
Photoluminescence
Low temperature

ABSTRACT

This article describes the results from low temperature studies of the photoluminescence (PL) from colloidal CdSe nanocrystals prepared by the hot injection method in liquid paraffin. The synthesized nanocrystals were taken from the reaction mixture at different time intervals, their sizes were all within the quantum confinement range, and showed the typical size-dependent UV–vis absorption, PL and Raman spectral characteristics. The PL spectra and their temperature dependences were measured from room temperature (295 K) down to temperatures as low as 15 K, demonstrating that the exciton PL transitions followed the Varshni equation. The thermal quenching activation energy below 100 K was relatively low, while the luminescence was strongly quenched as the temperature was increased above 100 K, probably pointing at change in the degree of carrier localization. The smallest (2.6 nm in size) CdSe nanocrystals isolated in the beginning of the nanocrystal growth had a relatively symmetric size distribution and showed a single exciton emission band, while the samples isolated at later stages of the growth

* Corresponding author.
** Corresponding author. Tel.: +359 2 8161 331.
E-mail addresses: epv@phys.uni-sofia.bg (E. Valcheva), g.g.yordanov@gmail.com (G. Yordanov).
[1] Present address: Imec, Kapeldreef 75, B-3001 Leuven, Belgium.

http://dx.doi.org/10.1016/j.colsurfa.2014.07.045
0927-7757/© 2014 Elsevier B.V. All rights reserved.

process showed negatively skewed asymmetric size distribution, indicating that the growth mechanism of nanocrystals could be explained by the model of Ostwald ripening. The obtained results are expected to be helpful for better understanding of the PL properties of quantum dots and their formation and growth in non-polar organic solvents.

© 2014 Elsevier B.V. All rights reserved.

1. Introduction

Semiconductor nanocrystals (monocrystals of sizes 2–10 nm in diameter), known also as quantum dots (QDs), are perspective inorganic fluorescent nanomaterials, which efficiently absorb and emit visible light at room temperature as a result of the quantum confinement of the exciton [1–3]. The size-dependent photoluminescence (PL), broad excitation spectra and resistance to photo-bleaching makes colloidal QDs quite attractive materials for applications in bioimaging and optoelectronics. For example, differently sized cadmium selenide (CdSe) nanocrystals emitting from blue to red can be used as fluorescent biolabels [4–6], components of light-emitting diodes [7], lasers [8], FRET sensors [9], recording of fluorescent images [10], luminescent ink-jet printing [11], etc. Therefore, achieving an effective control of the PL of QDs has been a major goal for scientists in the field of QDs synthesis and there are still unsolved issues of this problem.

The width of the absorption and emission bands in the QDs spectra is a result of homogeneous (thermal) and inhomogeneous broadening. The inhomogeneous broadening comes from the polydispersity of the nanocrystal size [12]. Therefore, the relative changes in the shape and the width of the PL bands during the growth of QDs can be used as an indication for changes in the nanocrystal size distribution [13]. PL studies can be more informative when performed at low temperatures, when the thermal broadening of the emission bands is minimized and the effect of quantum confinement is observed in its most clear form. Such studies for QDs prepared by colloidal chemical methods are rare, although they are quite popular for QDs prepared by physical methods (such as epitaxy). Most of the known low temperature PL studies of colloidal QDs include investigations of the exciton lifetimes and excitonic radiative decay [14,15], exciton fine structure [16], single dot spectroscopy [17], and quantum dots embedded in polymer matrices [18,19].

In this work, we report studies on the PL properties of colloidal CdSe QDs as a function of the temperature, in the range from 15 to 295 K. The nanocrystals were prepared by the hot injection method in liquid paraffin and were characterized by transmission electron microscopy, elemental analysis (EDX), UV–vis absorption, and PL and Raman spectroscopy. Measurements of the PL at low temperatures intended to reveal the temperature dependences of the energy of exciton radiative transitions in nanocrystals of CdSe of different average size. Measurements at different laser excitation power were also performed. Since the CdSe QDs samples were obtained at various stages of the nanocrystal growth, any changes in the shape of the PL bands could be indicative for changes in the nanocrystal size distribution during the growth process. The PL emission bands become narrower at low temperatures due to decrease of the thermal peak broadening, which facilitates the detection of nanocrystal subpopulations of different sizes in a heterogeneous sample. These studies, together with electron microscopy observations, could provide information about the processes that take place during the nanocrystal formation and growth by the hot injection method in liquid paraffin.

2. Experimental

2.1. Materials and reagents

Commercially available cadmium oxide (CdO, 99%) (Fluka), tributylphosphine (TBP, 97%) and selenium powder (Se, 99.5%) (Aldrich) were used in this study. Tributylphosphine selenide (TBP-Se) dissolved in liquid paraffin (0.127 M) was prepared as previously described [20]. Chloroform and methanol were of analytical reagent grade from Labscan Ltd. (Ireland). All other chemicals and solvents were of analytical grade and were used as received.

2.2. Synthesis of nanocrystals

Nanocrystals of CdSe were synthesized in hot liquid paraffin according to a previously reported method [20]. Briefly, cadmium stearate precursor was prepared in liquid paraffin (15 ml) from cadmium oxide (50 mg; 0.39 mmol) and stearic acid (1.6 g) at 200 °C. Tributylphosphine selenide precursor (1.0 ml) precursor was injected to the reaction mixture at 250–260 °C and nanocrystals of various sizes and optical properties were prepared by varying the reaction time. The change in the average nanocrystal size during synthesis was routinely measured by UV–vis absorption spectroscopy. For isolation of nanocrystals of a desired size, the reaction mixture (or a desired aliquot of it) was rapidly cooled to room temperature when the desired nanocrystal diameter was reached. Four batches of CdSe nanocrystals of various sizes were prepared by sampling at different time of nanocrystal growth: 10 s (CdSe-1), 20 s (CdSe-2), 40 s (CdSe-3), and 60 s (CdSe-4). The obtained nanocrystals were purified by repeated washing/centrifugation with toluene and extractions with chloroform/methanol (1:1). The purified nanocrystals were dried in a vacuum desiccator to obtain dried fine powders.

2.3. Structural characterization of nanocrystals

The obtained nanocrystals were observed by using a transmission electron microscope (TEM) JEM-2100F (JEOL) operated at 200 kV. The microscope was equipped with a probe for energy dispersive X-ray (EDX) spectroscopy.

The UV–vis absorption spectra of nanocrystals were recorded using a double-beam UV/Vis spectrophotometer UV-190 (Shimadzu) at room temperature (25 °C) in quartz cuvettes. Absorption spectra were measured in toluene, containing 1% TBP as a stabilizer. The average nanocrystal size was calculated from the position of the exciton absorbance maximum using empirical equations as previously described [21].

The X-ray powder diffraction (XRD) analysis was performed on a powder diffractometer Siemens D500 with CuKα-radiation within 2θ range 20°–80°, a step of 0.05° 2θ and counting time 5 s/step.

Micro-Raman spectra were recorded using a LabRAM HR800 spectrometer equipped with a cryogenic CCD detector. The laser excitation line is 633 nm of a HeNe laser. The resolution of the Raman spectra was ~1 cm^{-1}. All the measurements were performed at room temperature.

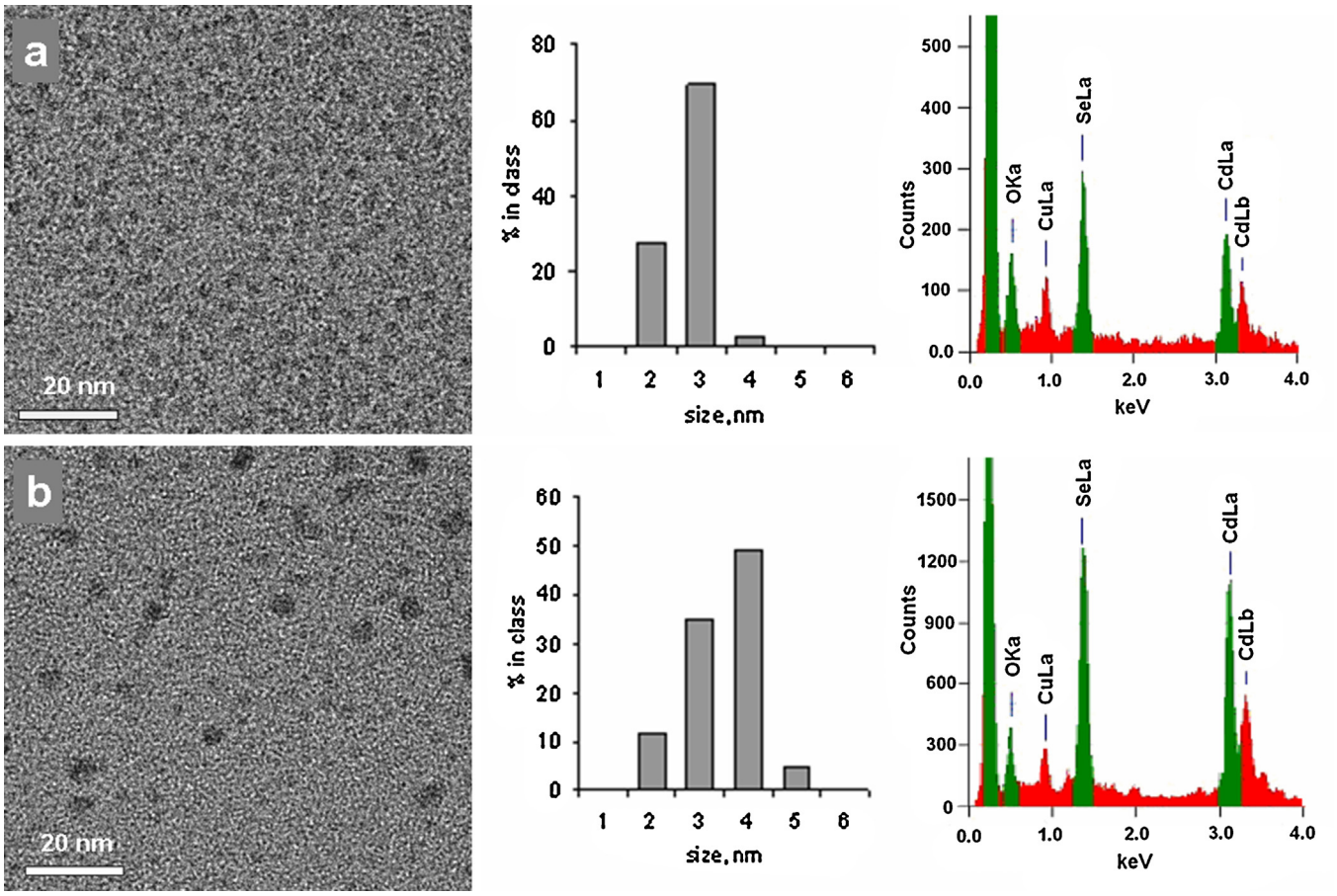

Fig. 1. Transmission electron microscopy (TEM; size bars represent 20 nm) images (left), size distributions (middle), and energy-dispersive X-ray (EDX) spectra (right) of CdSe nanocrystals from samples CdSe-1 (a), CdSe-4 (b).

2.4. Studies of the nanocrystal photoluminescence at low temperatures

For the PL experiments the nanocrystal powders were embedded into potassium bromide (KBr) tablets in order to be placed within the cryostat holder. For that purpose, dried nanocrystal powder (~20 mg) was homogenized with anhydrous powdered KBr (2 g) and compressed into tablets of suitable sizes (~2 cm in diameter; 5 mm thickness) by using a tablet press. The PL experiments were performed with a high resolution double monochromator (SPEX Model 1404, $f = 0.85$ m) equipped with Hamamatsu R943 PMTs (GaAs photocathode) with thermoelectric cooler and in photon counting mode. The samples were placed in a closed cycle ARS helium cryostat working in temperature interval from 295 down to 10 K. Argon laser emitting at a wavelength of 488 nm (2.54 eV) was used as an excitation source.

3. Results and discussion

3.1. Synthesis and structural characteristics of CdSe nanocrystals

Modern colloidal synthetic methods (such as the hot-injection method) allow the production of relatively monodisperse in size CdSe QDs [13,20,22,23]. However, optimization of the synthesis protocols is usually needed in order to find out the suitable conditions for the preparation of nanocrystals of the desired size distribution. The four batches of CdSe nanocrystals in our case were prepared by using the same synthetic protocol but varying only the reaction time – larger nanocrystals were obtained at longer reaction times. Investigations by transmission electron microscopy (TEM) revealed that the obtained nanocrystals were of spheroid shape (Fig. 1). Energy-dispersive X-ray (EDX) spectroscopy confirmed the elemental composition of nanocrystals, being composed of cadmium and selenium (Fig. 1; signals for other elements, such as copper, appear to be from the TEM grid). All samples contained oxygen peak in the EDX spectrum, which appears to be from the cadmium stearate precursor present in the samples. The presence of stearate was also confirmed by the XRD analysis (see below). TEM observation of the nanocrystals of smallest sizes (such as CdSe-1, see Table 1) indicated a relatively uniform size distribution, although the images were relatively unclear because the nanocrystal sizes were quite small (2.5–3.0 nm). The cadmium stearate present in the samples could also be a reason for the observed low resolution of TEM images. TEM images of larger nanocrystals (such as CdSe-4) were clearer, indicating negatively skewed asymmetric size distribution (Fig. 1b). The heterogeneity of these samples was confirmed also from the PL spectra measured at low temperatures (to be presented further) and was probably a result of Ostwald ripening during the formation of nanocrystals in the liquid paraffin medium (see the discussion in Sections 3.2 and 3.3). X-ray powder diffraction (Fig. 2) studies confirmed the nanocrystal size and the cubic crystal structure. The Cd-stearate precursor is used in excess and is difficult to be removed completely from the system. Therefore, all QD samples contain unreacted Cd-stearate. For example, the peaks at 22°, 23.7°, and 45° 2θ in the XRD pattern of sample CdSe-4 (Fig. 2) appeared to be from Cd-stearate precursor present in the sample. Diffraction peaks, characteristic for cubic phase, appeared at 2θ 25.5° (1 1 1), 42.2° (2 2 0) and 49.2° (3 1 1).

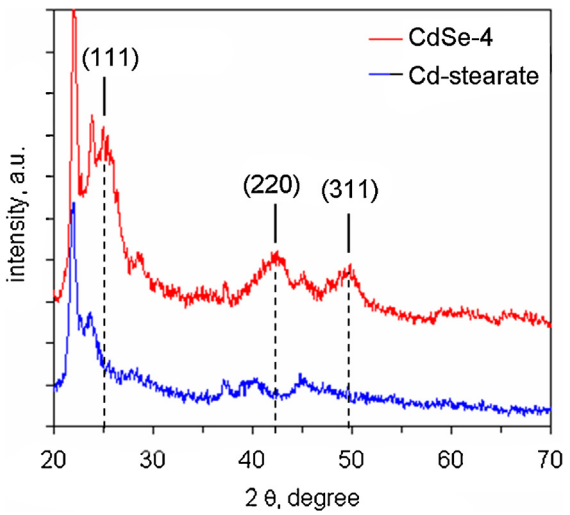

Fig. 2. XRD patterns of CdSe nanoparticles (sample CdSe-4) and cadmium stearate precursor. The peaks at 22°, 23.7°, and 45° 2θ in the XRD pattern of the CdSe-4 sample appear to be from Cd-stearate precursor present in the sample.

The lattice parameter (6.09 ± 0.04 Å) was close to that for the bulk cubic CdSe (6.05 Å [24]), indicating a similar X-ray density of the nanocrystals to that of the bulk material (our previous studies indicated that in some cases the X-ray density of nanocrystals could be higher than that of bulk material [25]). The diffraction peaks appeared broad due to the small size of nanocrystals (for example, fits with the Scherrer equation for the CdSe-4 sample in Fig. 2 indicated crystallite sizes of 3.8 ± 0.3 nm, which well corresponded to TEM observation, ca. 4 nm).

The UV–vis absorption spectra of the nanocrystal samples are shown in Fig. 3a. All spectra showed a characteristic absorption band in the visible region. The position (wavelength) of its maximum appeared to be size-depended as a result of the quantum confinement effect (the wavelength was shorter for smaller nanocrystals). The energy of the lowest excited state, $E(R)$, according to a simplified version of the effective mass model of Brus [26], is given by the following expression (Eq. (1)) that is valid for spherical nanocrystals of small radii R.

$$E(R) = E_g + \frac{h^2}{8mR^2} \quad (1)$$

Here, E_g is the energy band gap for the bulk semiconductor, h is the Planck constant, m is the effective mass of the exciton. However, the calculated energy $E(R)$ for nanocrystals of a given radius R (using Eq. (1)) is usually larger than the experimentally estimated values, which leads to overestimated nanocrystal sizes if Eq. (1) is used for calculation of the nanocrystal size from the UV–vis absorption spectra. This represents a significant problem for nanocrystal synthesis, where the size is routinely estimated from the absorption spectra measured during the nanocrystal growth process. Therefore, empirical polynomials relating the peak absorbance wavelength and nanocrystal sizes have been derived for various Cd-based quantum dots. The average nanocrystal sizes in our studies were calculated from the position (wavelength) of the peak absorbance

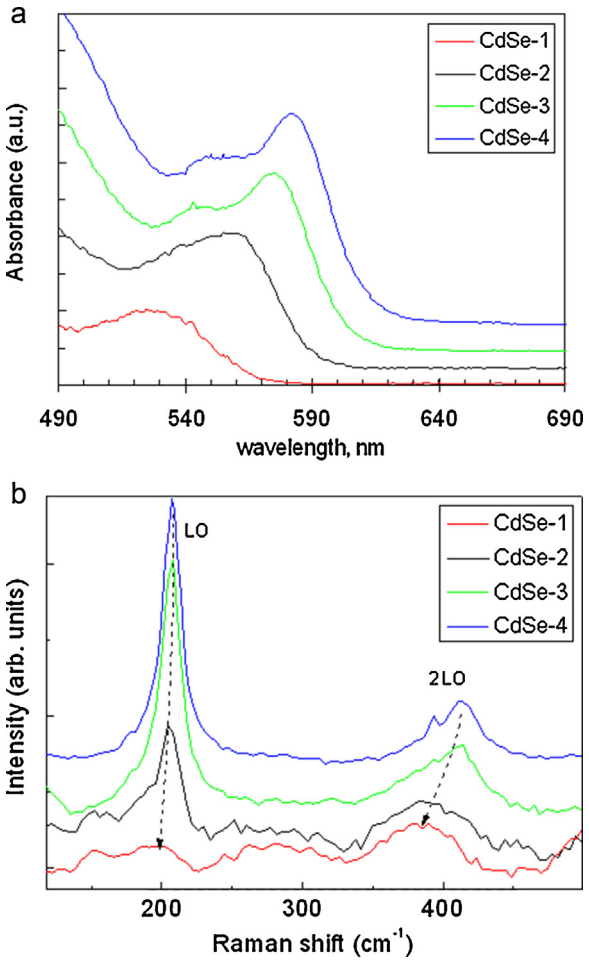

Fig. 3. (a) UV–vis absorption spectra, and (b) Raman spectra of the obtained QDs. The spectra are given with offset for clarity.

wavelength (λ_{AB}) in the visible spectrum by using such an empirical formula previously derived by Yu et al. [21] (Eq. (2)).

$$D = (1.6122 \times 10^{-9})\lambda^4 - (2.6575 \times 10^{-6})\lambda^3 + (1.6242 \times 10^{-3})\lambda^2 - 0.4277\lambda + 41.57 \quad (2)$$

Here, λ is the peak absorbance wavelength (in nm) (λ_{AB} in Table 1), measured at room temperature, and D is the average nanocrystal diameter (in nm). The energy of the lowest excited state, E_{AB}, was size-dependent (as discussed above) and was calculated from the experimentally obtained wavelength of the absorbance maximum λ_{AB}. The obtained data for the wavelengths of absorbance (λ_{AB}) and PL (λ_{PL}) maxima in the nanocrystal spectra measured at room temperature (295 K), calculated nanocrystal sizes and energies of the lowest excited states are summarized in Table 1. It should be noted that the absorption spectra of samples CdSe-2, CdSe-3 and CdSe-4 had a "shoulder" on the short wavelength side of the spectrum while the smallest size dots spectrum

Table 1
Peak absorbance (λ_{AB}) and emission (λ_{PL}) wavelengths (measured at 295 K), sizes and calculated energies ($E_{AB} = 1239.85/\lambda_{AB}$; $E_{PL} = 1239.85/\lambda_{PL}$) for the five batches of quantum dots used for the PL studies (the average size of CdSe QDs was calculated from λAB and well correlated with TEM data). The Stokes shift was calculated as E_{AB}–E_{PL}.

Sample	λ_{AB} (nm)	Size (nm)	λ_{PL} (nm)	E_{AB} (eV)	E_{PL} (eV)	Stokes shift (eV)
CdSe-1	526	2.6	556	2.357	2.230	0.127
CdSe-2	559	3.2	580	2.218	2.138	0.080
CdSe-3	574	3.6	598	2.160	2.073	0.087
CdSe-4	582	3.9	601	2.130	2.063	0.067

only did not show it. Empirical polynomials (such as Eq. (2)) should be verified for each particular QDs. Our previous studies [20] have confirmed the validity of Eq. (2) for QDs prepared by the paraffin method used in this current study. Also, QDs sizes calculated with Eq. (2) were consistent with data from TEM observation and XRD studies. For example, the calculated nanoparticle size (by using Eq. (2)) for CdSe-4 was 3.9 nm, which corresponded well to the size obtained from XRD (3.8 nm) and TEM (ca. 4 nm) for the same sample.

The Raman spectra of the CdSe nanocrystals are shown in Fig. 3b – CdSe-1 (with a LO peak at 200.0 cm^{-1}), CdSe-2 (with a peak at 205.7 cm^{-1}), CdSe-3 (with a peak at 207.09 cm^{-1}) and CdSe-4 (with a peak at 207.5 cm^{-1}). The observed peak values were close to that of the bulk CdSe (210 cm^{-1}). The shift toward lower frequencies was found to be size-dependent and could be attributed to the phonon quantum confinement that is typical for semiconductor nanocrystals within these size ranges [27].

3.2. Low temperature photoluminescence studies

The so-called normal band-edge photoluminescence of QDs is a result of radiative decay of an electron that has been excited from the valence to the conduction band and therefore its energy is a function of the band gap [28]. The optical energy transitions in the spectra of an ensemble of QDs at room temperature are not discrete but appear as absorbance and PL bands. The width of these bands is a result of homogeneous (thermal) and inhomogeneous broadening, the latter coming from the polydispersity of nanocrystal size [12]. Crystal defects could introduce potential energy states in the band gap and excited electrons could be trapped at this state. The radiative decay of electrons trapped at surface states to the ground state causes the so-called trap-state emission, which appears in the spectrum at longer wavelengths than the band-edge emission [26,28]. Therefore, PL appears as one of the most sensitive methods for analysis of QDs, which allows one to obtain information and to discriminate between different recombination processes, related with various recombination centers in the nanocrystal lattice. In the case of QDs PL measurements could provide information about the energy levels and quantum confinement effects. The correct interpretation of the PL peaks could also provide information about the existence of excitons, the morphology of the hetero-interface, the presence of defects and impurities, etc. As mentioned above, the energy of the PL peak, its shape and width could provide information about the average size and size distribution of the nanocrystals. Since the homogeneous (thermal) broadening of the PL bands could be minimized at lower temperatures, we performed PL measurements at low temperatures (down to 15 K) in order to investigate the temperature dependence of the PL peak energy and to evaluate the size homogeneity of the samples.

Fig. 4a and b represents PL-spectra of the four CdSe nanocrystal samples at room temperature 295 K and at 15 K, respectively. The spectra are normalized to the highest energy peak and the PL intensity is presented in logarithmic scale to be easily observed. Most of the emission spectra show two shoulders at the high-energy side visible also in the room temperature spectra but more pronounced at low temperatures, and a low intensity shoulder at the low energy side.

The most intensive PL peak for the four different nanocrystal sizes was shifted toward higher energies than the band gap of the bulk CdSe (1.74 eV at room temperature). The PL maximum shifts toward higher energies with decreasing of the nanocrystal size, which is a characteristic observation of quantum-size effects for nanocrystals of sizes that are smaller than the exciton Bohr radius (~5.6 nm for CdSe). For the CdSe nanocrystals under investigation we found an empirical relation (based on the data in Table 1)

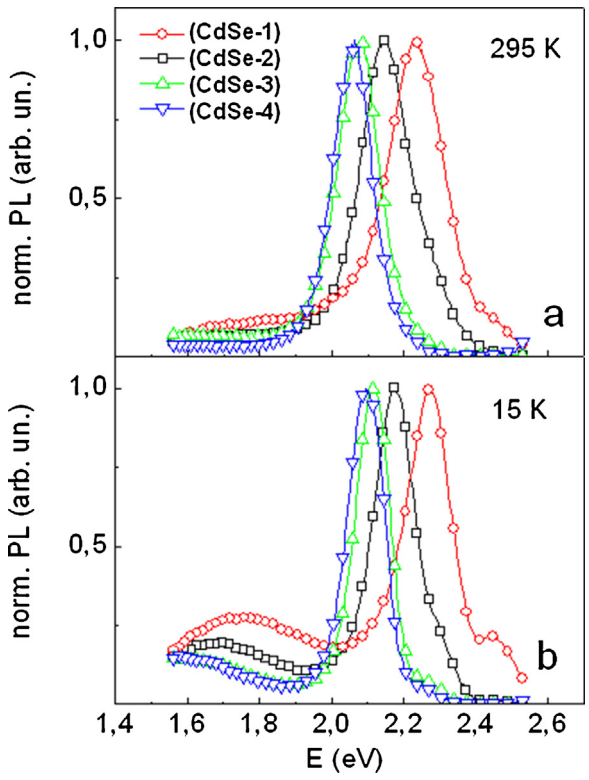

Fig. 4. Normalized PL-spectra of the four CdSe QD-samples at 295 K (top) and 15 K (bottom). To take into account the different features, the logarithmic PL curves at each temperature were deconvoluted with a sum of Gaussians (Figs. 5 and 6).

between the position of the PL peak (λ_{PL}) and the average nanoparticle size (Eq. (3)).

$$D = (1.087 \times 10^{-4})\lambda_{PL}^2 - (9.982 \times 10^{-2})\lambda_{PL} + (24.53) \quad (3)$$

Here, λ_{PL} is the PL peak wavelength (in nm), measured at 295 K, and D is the average nanocrystal diameter (in nm).

The spectra of samples CdSe-3 and CdSe-4 are quite similar probably due to the similar sizes of the respective nanocrystals (see Table 1). This observation also corresponds to the relative similar UV–vis absorption spectra of samples CdSe-3 and CdSe-4 (Fig. 3a).

The temperature dependent PL spectra for one of the samples (CdSe-2) measured from 15–295 K are given in Fig. 5a. Fig. 5b illustrates the best fit of the low temperature (15 K) spectrum with five Gaussians. The peaks are indexed as p0 ÷ p4. The purpose of this fitting procedure was to determine the nature of the respective energy transitions.

Fig. 6a and b shows similar temperature dependences measured for sample CdSe-1. In the latter case, the spectrum was fitted with a combination of four Gaussians (p1 was actually missing in this case). The spectra of CdSe-3 and CdSe-4 are best fitted with five Gaussians similar to CdSe-2.

In order to clarify the origin of the constituent peaks of the spectra the temperature dependences of the peak positions (the peak energy) of p0, p1 and p2 are presented in Fig. 7 for CdSe-2. The corresponding dependences for CdSe-1, CdSe-3 and CdSe-4 (not shown here) reveal similar character.

Peak p0 does not depend on the temperature and is situated around 500 nm for all the four groups of samples (Fig. 7a). Its nature is currently unclear. The temperature dependences of p1 and p2 correspond to the expected behavior for exciton transitions. The observation of two exciton peaks, p1 and p2 in the case of CdSe-2 (Figs. 5 and 7) could be interpreted as an indication for the presence of two subpopulations of exciton states, corresponding to

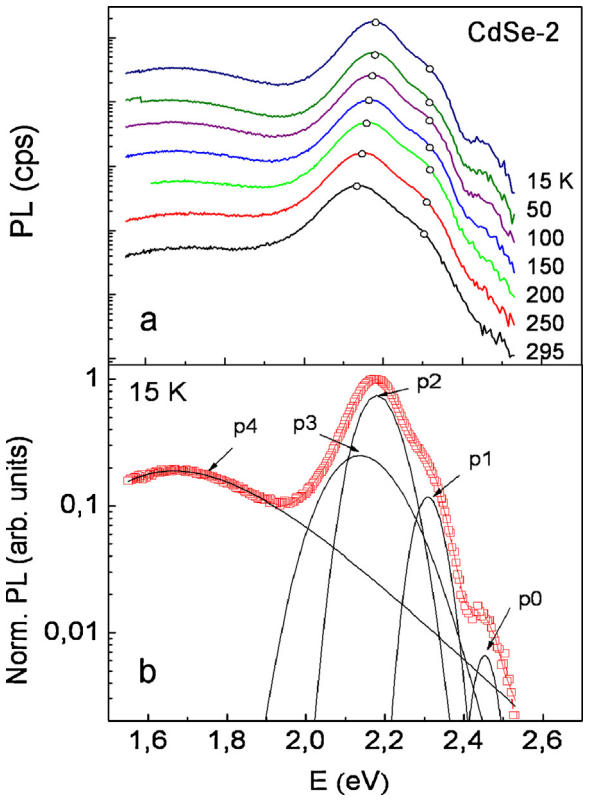

Fig. 5. (a) PL-spectra of sample CdSe-2 at various temperatures (from 15 to 295 K, log scale; offset for clarity); (b) PL spectrum of sample CdSe-2 (at 15 K, log scale) fitted with five Gaussians.

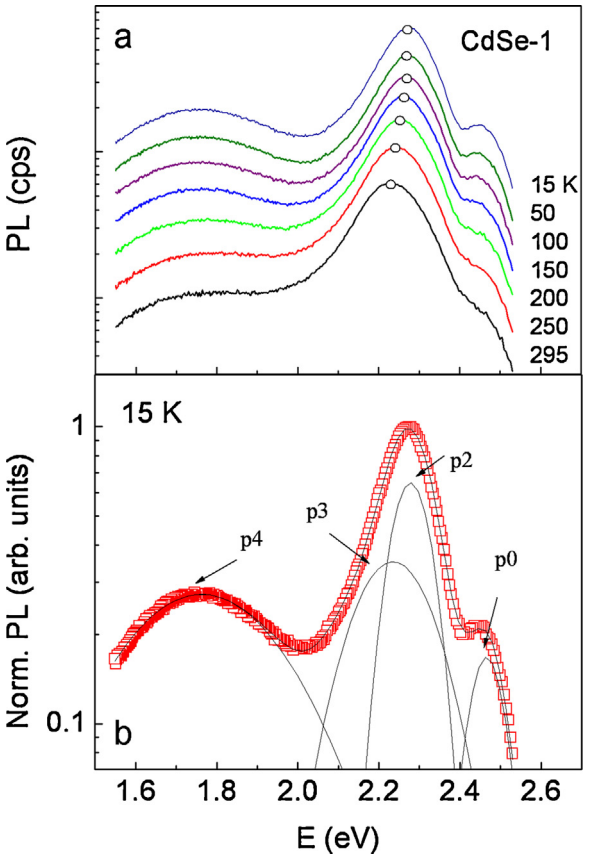

Fig. 6. (a) Temperature dependence of the PL-spectrum of sample CdSe-1 in the temperature interval from 15 to 295 K, log scale; offset for clarity; (b) PL-spectrum of sample CdSe-1 (at 15 K) fitted with four Gaussians.

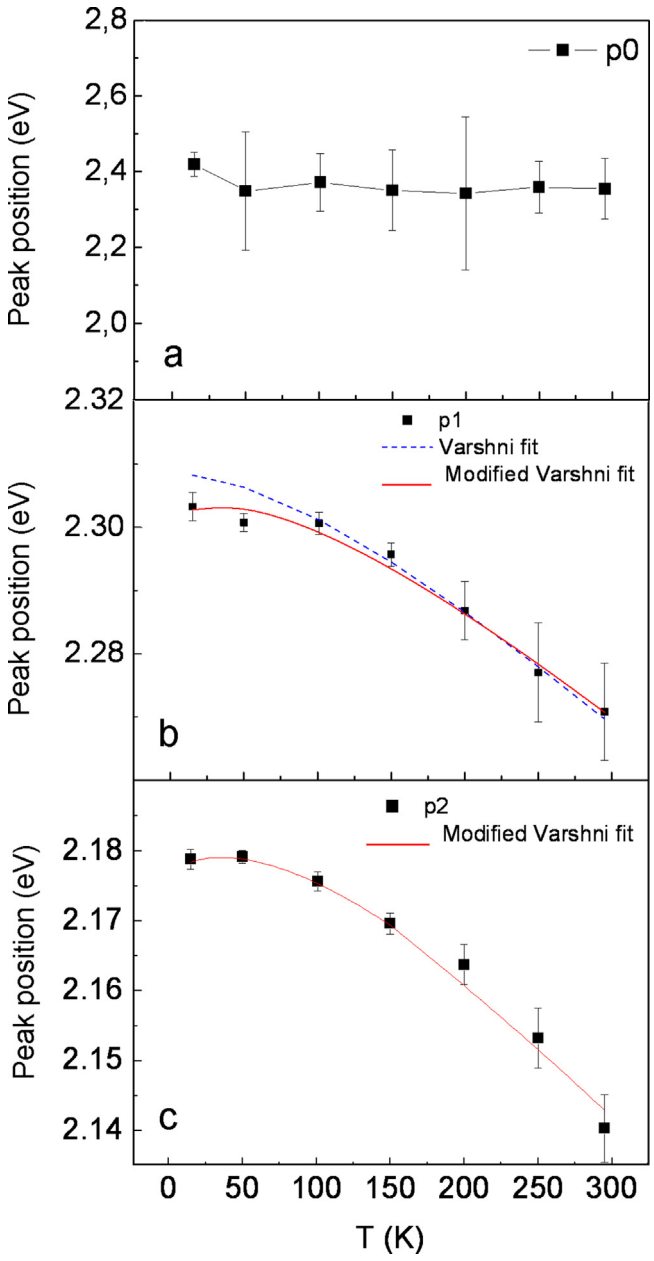

Fig. 7. Temperature dependences of the peak position (energy) of p0 (a), p1(b), and p2 (c) from Fig. 5 for CdSe-2.

nanocrystals of average sizes 2.6 and 3.2 nm, respectively, the latter of which is the predominant one. The energy shift between them is 0.125 eV, which value together with the relatively larger FWHM (full width at half maximum) (70 ÷ 100 meV) are thought to support this suggestion. In the cases of samples CdSe-3 and CdSe-4 two peaks are also observed, with a similar behavior to that of p1 and p2. Additionally, all samples reveal low energy shoulder of lower intensity and larger FWHM labeled with p3. However, the relative intensities of these three emission peaks might not be proportional to the number of QDs in the respective subpopulations because of at least two reasons: (i) the PL quantum yield of QDs may depend on many different factors [13], and (ii) the emission from the largest dots in the size distributions might be enhanced by Förster resonant energy transfer (FRET) from smaller dots [29]. The latter could be a possible explanation for the observation of peak p3 in the spectra of all four different samples if it is ascribed to subpopulation of larger size nanocrystals. The existence of a

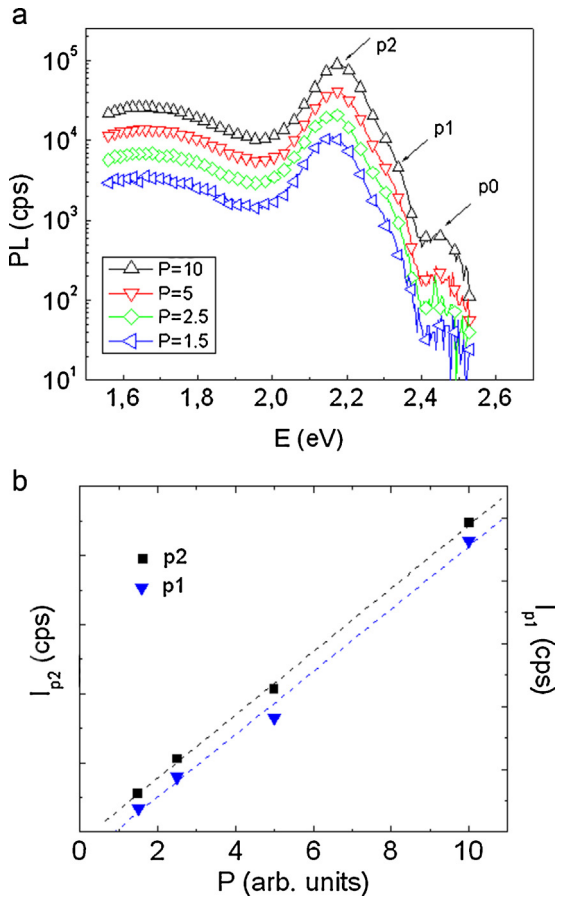

Fig. 8. PL spectra of CdSe-2 at $T = 20$ K (a) and dependence of the PL intensity of peaks p1 and p2 on the laser intensity (b). The laser intensity (P) is given in arbitrary units.

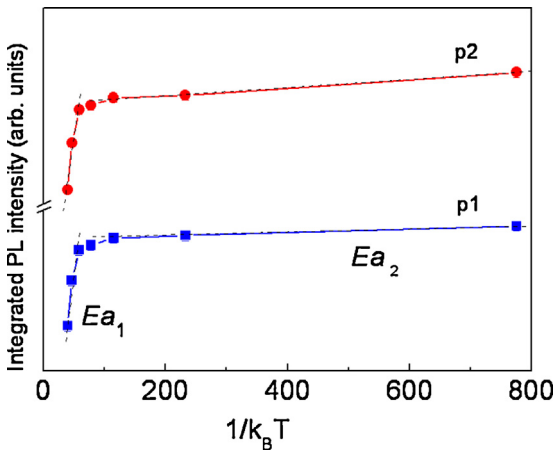

Fig. 9. Arrhenius plots – integrated PL intensity variation of the exciton transition as a function of the reciprocal temperature for CdSe-2, peaks p1 and p2.

subpopulation of smaller nanocrystals could also be associated with the appearance of a "shoulder" on the shorter wavelength side of the main absorbance band in the UV–vis spectra for CdSe-2, CdSe-3 and CdSe-4 shown in Fig. 3. Finally, the peak p4 is ascribed to surface-state-mediated recombination [30,31].

Additional low temperature measurements were performed at various intensities of the laser excitation light by using suitable filters for changing the intensity of the laser light. The obtained results for the CdSe-2 are presented in Fig. 8. The observed linear dependence for peaks p1 and p2 on the intensity of the laser excitation beam confirms their excitonic character [32].

The temperature dependence of the energy gap of bulk semiconductors is known as the Varshni relation [33] (Eq. (4)).

$$E_g(T) = E_g(0) - \alpha \frac{T^2}{T+\beta} \tag{4}$$

Here, $E_g(0)$ is the energy gap at 0 K, α is the temperature coefficient, and the value of β is close to the Debye temperature of the material. The experimental data for the four QDs were fitted to the Varshni relation. Eq. (4) fits very well the high temperature range 100–295 K (Fig. 7 b and c, fits for CdSe-2) consistent with the known temperature dependence of bulk semiconductor band gap. However, at temperatures lower than 100 K obviously the PL energies deviate from Varshni equation, plateau and even "S-shape" behavior is observed pointing out at involvement of different mechanism connected with relaxation dynamics of localized carriers and confinement. Indeed, better fits in the low temperature range were obtained (Fig. 7b and c) if a modified equation (Eq. (4a)) was used:

$$E_g(T) = E_g(0) - \alpha \frac{T^2}{T+\beta} - \frac{\sigma^2}{kT}, \tag{4a}$$

where the parameter σ represents a measure of the depth of localization potentials [34] and k is the Boltzmann's constant. Similar behavior is observed in quantum dots and in quantum well structures, where it is explained in terms of localized exciton freeze-out at low temperatures, followed by the onset of thermalization of excitons with increasing temperature [34].

The values for the fitting parameters for all samples are shown in Table 2. The fitted parameters are consistent with the values given in the literature for bulk CdSe: $(2.8–4.1) \times 10^{-4}$ eV/K for α and (181–315) K for β (Ref. [35]). The σ values reveal localization energy $\sim 2 \div 4$ meV from fitting the transition peaks.

Further we studied the intensity variations of all peaks as function of temperature to get a clear picture of the thermally induced processes. The Arrhenius plots of the integrated PL intensities from the exciton-transition related PL emission as a function of inverse temperature are shown in Fig. 9 for sample CdSe-2. The plots suggest the existence of two relaxation processes having different activation energies the dependence being of the form [36]:

$$I(T) = \frac{I_0}{1 + C_1 \exp(-Ea_1/kT) + C_2 \exp(-Ea_2/kBT)}, \tag{5}$$

Table 2
Fitting parameters from the Varshni equation (Eq. (3)) describing the temperature dependence of the main exciton transition peak (p2). The correlation coefficient (R^2) for each fit is also given.

Sample	$E_g(0)$ (eV)		α (eV/K)	β (K)	R^2	σ (meV)
CdSe-1	p2	2.281 ± 0.001	$(2.7 \pm 0.1) \times 10^{-4}$	230 ± 20	0.994	2.1 ± 0.7
	p2	2.185 ± 0.002	$(2.5 \pm 0.2) \times 10^{-4}$	220 ± 20	0.995	2.8 ± 0.8
CdSe-2	p1	2.308 ± 0.007	$(2.4 \pm 0.3) \times 10^{-4}$	255 ± 20	0.994	4.6 ± 0.7
	p2	2.123 ± 0.001	$(2.9 \pm 0.1) \times 10^{-4}$	320 ± 20	0.974	2.5 ± 0.8
CdSe-3	p1	2.278 ± 0.003	$(4.8 \pm 0.4) \times 10^{-4}$	284 ± 20	0.975	4.5 ± 0.7
CdSe-4	p2	2.104 ± 0.001	$(2 \pm 0.1) \times 10^{-4}$	220 ± 20	0.986	2.7 ± 0.8
	p1	2.264 ± 0.002	$(4.1 \pm 0.3) \times 10^{-4}$	255 ± 20	0.988	4.3 ± 0.5

Table 3
Values of the low- and high-temperature activation energies $Ea_{1,2}$.

Sample	Ea_1 (meV) (at $T < 100$ K)		Ea_2 (meV) (at $T > 100$ K)	
	p2	p1	p2	p1
CdSe-1	0.34	–	39	–
CdSe-2	0.73	0.78	10.6	16.9
CdSe-3	0.21	0.11	7.3	3.1
CdSe-4	0.13	0.17	9.5	8.8

where $Ea_{1,2}$ are the activation energies of the low- and high-temperature quenching processes, $C_{1,2}$ are constants independent of temperature and I_0 is the intensity at $T = 0$ K. The fits to the experimental data by using Eq. (5) reveal the thermal quenching activation energies $Ea_{1,2}$ (Table 3) related to the depth of the quantum-well confining potential for the carriers contributing to nonradiative processes in the different temperature ranges. The activation energies below 100 K are very low while the luminescence is strongly quenched as the temperature is increased above 100 K probably pointing at change in the degree of carrier localization. These energies vary also from dot to dot as a consequence of quantum confinement. The finding that both the observed flattening of the PL peak energy in Fig. 7 and the PL quenching, related to lower activation energy Ea_1 occur in the same temperature range (15–100 K) suggests that these two phenomena are correlated. Assuming that the probability of radiative process in quantum-well structure is independent of temperature the difference between the thermal activation energies Ea_1 and Ea_2 might be due to different degrees of carrier localization.

3.3. Model of CdSe nanocrystal growth in liquid paraffin

Photoluminescence measurements appeared to be a more sensitive approach for detection of heterogeneity in the size distribution than TEM, especially for the smallest nanocrystals, whose size was comparable with the size resolution limit of the TEM technique. Room temperature measurements of the PL may not always reveal the existence of subpopulations of nanocrystals within an ensemble because of the thermal (homogeneous) PL peak broadening. It appears that in the beginning of the nanocrystal growth process there were nanocrystals of uniform size distribution and the size heterogeneity (the observation of a second subpopulation of smaller nanocrystals together with the basic component) appeared in the later stages of the nanocrystal growth. Other authors who have previously obtained CdSe QDs samples with two dominant sizes (showing a double peak behavior) have suggested a second nucleation step and/or aggregated type of growth [37]. These authors reported a heterogeneous nanocrystal growth regime, during which nanoparticles with well-defined and very different sizes could coexist in the solution. They found that the average size and size distribution of the nanoparticles was primarily not controlled by the usual focusing/defocusing (Ostwald ripening), rather by the formation of "magic" sized particles.

However, our data are more likely to be explained by the model of Ostwald ripening. This model of the growth kinetics of QDs in the conditions of the hot-injection synthesis has been described by Talapin et al. [38]. According to this model, the average size and size distribution of the QDs are determined by the growth and the dissolution kinetics. In Ostwald ripening, the largest particles in the ensemble continue to grow and the smallest dissolve. Between these two cases there are particles having a nearly zero growth rate [36]. However, a general analytical solution describing all processes during the evolution of the entire ensemble could not be obtained and Ref. [38] describes the application of Monte Carlo simulation in order to obtain statistical information about the ensemble behavior. This theoretical approach has shown that an initially symmetric normal particle size distribution evolves in time (during the nanocrystal growth) toward an asymmetric, negatively skewed one. The nanocrystals having a nearly zero growth rate were situated at the left part (toward smaller particles) of the entire ensemble at all stages of growth [38]. As seen, this model quite well describes our experimental data, particularly the initial symmetric size distribution that evolves toward a negatively skewed asymmetric one. In another report, Talapin et al. [39] proposed that the nanocrystal fraction with the best surface quality and, thus, with the most efficient PL quantum yield corresponds to the particle size with the smallest net growth (i.e., the particles with a nearly zero growth rate that are situated at the left part of the entire ensemble). All these findings appear to be important and should be taken into account in future studies intended to reveal more details on the mechanisms of formation and growth of colloidal nanocrystals.

4. Conclusions

In this paper we reported results from low temperature PL studies on colloidal CdSe nanocrystals, prepared by the hot injection method in liquid paraffin. The average nanocrystal size (from 2.6 to 4.3 nm for the various samples) was determined from UV–vis absorption spectra and TEM observations. The temperature dependencies (from 15 to 295 K) of the exciton PL transitions were found to follow the Varshni equation. At temperatures lower than 100 K the PL energies deviated from Varshni equation and plateau behavior was observed pointing out at involvement of different mechanism connected with relaxation dynamics of localized carriers and confinement. The thermal quenching activation energy below 100 K was relatively low, while the luminescence was strongly quenched as the temperature was increased above 100 K, probably pointing at change in the degree of carrier localization. The CdSe nanocrystals of smallest size (2.6 nm) were found to be of uniform size distribution possessing a single emission band in the PL spectrum. However, the CdSe samples obtained at later stages of growth, showed an asymmetrical size distribution and PL from a subpopulation of smaller nanocrystals found together with the larger ones. We hope that the data reported here could be helpful for better understanding of the nanocrystal growth of CdSe nanocrystals and their PL properties.

Acknowledgments

This research was partially supported by the Scientific Research Fund (project ref. number 16/2007). G.Y. is thankful to CMST COST Action CM1101. The technical support from Dr. Anton Apostolov (Sofia University, Faculty of Chemistry and Pharmacy) with XRD measurements is greatly acknowledged.

References

[1] A.L. Rogach (Ed.), Semiconductor Nanocrystal Quantum Dots: Synthesis, Assembly, Spectroscopy and Applications, Springer-Verlag, Wien, 2008.
[2] A.D. Yoffe, Semiconductor quantum dots and related systems: electronic, optical luminescence and related properties of low dimensional systems, Adv. Phys. 42 (1993) 173–266.
[3] S.V. Gaponenko, Optical Properties of Semiconductor Nanocrystals, Cambridge University Press, Cambridge, 2005.
[4] W. Chan, D. Maxwell, X. Gao, R. Bailey, M. Han, S. Nie, Luminescent quantum dots for multiplexed biological detection and imaging, Curr. Opin. Biotechnol. 13 (2002) 40–46.
[5] F. Pinaud, X. Michalet, L. Bentolila, J. Tsay, S. Doosel, J. Li, G. Iyer, S. Weiss, Advances in fluorescence imaging with quantum dot bio-probes, Biomaterials 27 (2006) 1679–1687.
[6] T. Jamieson, R. Bakhshi, D. Petrova, R. Pocock, M. Imani, A. Seifalian, Biological applications of quantum dots, Biomaterials 28 (2007) 4717–4732.
[7] M. Schlamp, X. Peng, A.P. Alivisatos, Improved efficiencies in light emitting diodes made with CdSe(CdS) core/shell type nanocrystals and a semiconducting polymer, J. Appl. Phys. 82 (1997) 5837–5842.

[8] V. Klimov, A. Mikhailovsky, S. Xu, A. Malko, J. Hollingsworth, C. Leatherdale, H. Eisler, M.G. Bawendi, Optical gain and stimulated emission in nanocrystal quantum dots, Science 290 (2000) 314–317.
[9] I.L. Medintz, H. Mattoussi, Quantum dot-based resonance energy transfer and its growing application in biology, Phys. Chem. Chem. Phys. 11 (2009) 17–45.
[10] S. Maenosono, C. Dushkin, S. Saita, Y. Yamagushi, Optical memory media based on excitation-time dependent luminescence from a thin film of semiconductor nanocrystals, Jpn. J. Appl. Phys. 39 (2000) 4006–4012.
[11] E. Binetti, C. Ingrosso, M. Striccoli, P. Cosma, A. Agostiano, J.Y. Kim, J. Brugger, M.L. Curri, Conjugated polymer and luminescent nanocrystals for ink-jet printing, AIP Conf. Proc. 1255 (2010) 89–91.
[12] A.P. Alivisatos, A. Harris, N. Levinos, M. Steigerwald, L. Brus, Electronic states of semiconductor clusters: homogeneous and inhomogeneous broadening of the optical spectrum, J. Chem. Phys. 89 (1988) 4001–4011.
[13] L. Qu, X. Peng, Control of photoluminescence properties of CdSe nanocrystals in growth, J. Am. Chem. Soc. 124 (2002) 2049–2055.
[14] M. Califano, A. Franceschetti, A. Zunger, Temperature dependence of excitonic radiative decay in CdSe quantum dots: the role of surface hole traps, Nano Lett. 5 (2005) 2360–2364.
[15] C. de Mello Donegá, M. Bode, A. Meijerink, Size- and temperature-dependence of exciton lifetimes in CdSe quantum dots, Phys. Rev. B 74 (2006), Art. no. 085320.
[16] D.J. Norris, A.L. Efros, M. Rosen, M.G. Bawendi, Size dependence of exciton fine structure in CdSe quantum dots, Phys. Rev. B 53 (1996) 16347–16354.
[17] S.A. Empedocles, D.J. Norris, M.G. Bawendi, Photoluminescence spectroscopy of single CdSe nanocrystallite quantum dots, Phys. Rev. Lett. 77 (1996) 3873–3876.
[18] D. Valerini, A. Cretí, M. Lomascolo, L. Manna, R. Cingolani, M. Anni, Temperature dependence of the photoluminescence properties of colloidal CdSeZnS core/shell quantum dots embedded in a polystyrene matrix, Phys. Rev. B 71 (2005), Art. no. 235409.
[19] T.T.K. Chi, U.T.D. Thuy, N.Q. Liem, M.H. Nam, D.X. Thanh, Temperature-dependent photoluminescence and absoprtion of CdSe quantum dots embedded in PMMA, J. Korean Phys. Soc. 52 (2008) 1510–1513.
[20] G. Yordanov, H. Yoshimura, C. Dushkin, Fine control of the growth and optical properties of CdSe quantum dots by varying the amount of stearic acid in a liquid paraffin matrix, Colloids Surf. A 322 (2008) 177–182.
[21] W. Yu, L. Qu, W. Guo, X. Peng, Experimental determination of the extinction coefficient of CdTe, CdSe, and CdS nanocrystals, Chem. Mater. 15 (2003) 2854–2860.
[22] W. Yu, X. Peng, Formation of high-quality CdS and other II–VI semiconductor nanocrystals in noncoordinating solvents: tunable reactivity of monomers, Angew. Chem. Int. Ed. 41 (2002) 2368–2371.
[23] L. Qu, Z.A. Peng, X. Peng, Alternative routes toward high quality CdSe nanocrystals, Nanoletters 1 (2001) 333–337.
[24] O. Madelung, M. Schlz, H. Weiss (Eds.), Numerical Data and Functional Relationships in Science and Technology. Landolt-Borstein, vol. 17, Springer, Berlin, 1982.
[25] B. Bochev, G. Yordanov, Room temperature synthesis of thioglycolate-coated zinc sulfide (ZnS) nanocrystals in aqueous medium andtheir physicochemical characterization, Colloids Surf. A 441 (2014) 84–90.
[26] M.G. Bawendi, M.L. Steigerwald, L.E. Brus, The quantum mechanics of larger semiconductor clusters (quantum dots), Annu. Rev. Phys. Chem. 41 (1990) 477–496.
[27] A. Kelley, Q. Dai, Z. Jiang, J. Baker, D. Kelley, Resonance Raman spectra of wurtzite and zinc blende CdSe nanocrystals, Chem. Phys. 422 (2013) 272–276.
[28] M. Nirmal, L. Brus, Luminescence photophysics in semiconductor nanocrystals, Acc. Chem. Res. 32 (1999) 407–414.
[29] C.R. Kagan, C.B. Murray, M.G. Bawendi, Long-range resonance transfer of electronic excitations in close-packed CdSe quantum-dot solids, Phys. Rev. B 54 (1996) 8633–8643.
[30] G. Schmid (Ed.), Nanocrystals: From Theory to Application, Wiley–VCH, Weinheim, 2004 (and references therein).
[31] N. Chestnoy, T.D. Harris, R. Hull, L.E. Brus, J. Phys. Chem. 90 (1986) 3393.
[32] T. Schmidt, K. Lischka, W. Zulehner, Excitation-power dependence of the near-band-edge photoluminescence of semiconductors, Phys. Rev. B 45 (1992) 8989–8994.
[33] Y.P. Varshni, Temperature dependence of the energy gap in semiconductors, Physica 34 (1967) 149–154.
[34] J.H. Park, D.G. Choi, T.K. Lee, Eunsoon Oh, Sanghoon Lee, J.K. Furdyna, Localization and interdot carrier transfer in CdSe and CdZnMnSe quantum dots determined by cw and time-resolved photoluminescence, Appl. Phys. Lett. 90 (2007) 201916.
[35] K.H. Hellwege (Ed.), Numerical Data and Functional Relationship in Science and Technology. Hellwege, Landolt-Börnstein, New Series, Group III, vol. 17, Pt. B, Springer-Verlag, Berlin, 1982.
[36] Y.-H.O. Wu, K. Arai, T. Yao, Phys. Rev. B 53 (1996) R10485.
[37] C. Tuinenga, J. Jasinski, T. Iwamoto, V. Chikan, In situ observation of heterogeneous growth of CdSe quantum dots: effect of indium doping on the growth kinetics, ACS Nano 2 (2008) 1411–1421.
[38] D. Talapin, A. Rogach, M. Haase, H. Weller, Evolution of an ensemble of nanoparticles in a colloidal solution: theoretical study, J. Phys. Chem. B 105 (2001) 12278–12285.
[39] D. Talapin, A. Rogach, E. Shevchenko, A. Kornowski, M. Haase, H. Weller, Dynamic distribution of growth rates within the ensembles of colloidal II–VI and III–V semiconductor nanocrystals as a factor governing their photoluminescence efficiency, J. Am. Chem. Soc. 124 (2002) 5782–5790.